Appl Phys A (2013) 110:743–749
DOI 10.1007/s00339-012-7135-8

Applied Physics A
Materials Science & Processing

Local near field assisted ablation of fused silica

An experimental and theoretical study

Abdul Aleem Jamali · Bernd Witzigmann · Rodica Morarescu · Thomas Baumert · Frank Träger · Frank Hubenthal

Received: 1 June 2011 / Accepted: 3 August 2012 / Published online: 29 August 2012

Abstract In this contribution we present recent experimental and theoretical results on local near-field assisted laser ablation. Along these lines, we have generated sub-diffraction sized nanostructures on fused silica substrates, exploiting the local near fields of highly ordered triangular gold nanoparticle arrays generated by nanosphere lithography. After preparation, the nanoparticle arrays were irradiated with a single 35 fs long laser pulse with a central wavelength of $\lambda = 790$ nm. The pulse energy was set to $E = 3.9$ μJ, resulting in a fluence well below the ablation threshold of the fused silica substrates. In addition, 3D electromagnetic simulations using a finite integration technique in time domain have been performed. The simulations demonstrate that indeed the local field in the vicinity of the tips of the triangular nanoparticles overcome the ablation threshold and easily explain the generated nanostructures. Most importantly, the simulations show, that higher order modes contribute to the ablation process. These modes cause ablation along the side edges of the nanoparticles. Finally, we demonstrate, that the optical properties of the triangular nanoparticles, which can be tuned by their morphology, are crucial parameters for the generation of the ablation structures.

A.A. Jamali · B. Witzigmann
Computational Electronics and Photonics Group and Center for Interdisciplinary Nanostructure Science and Technology—CINSaT, University of Kassel, Wilhelmshöher Allee 71, 34121 Kassel, Germany

R. Morarescu · T. Baumert · F. Träger · F. Hubenthal (✉)
Department of Physics and Center for Interdisciplinary Nanostructure Science and Technology—CINSaT, University of Kassel, Heinrich-Plett-Str. 40, 34132 Kassel, Germany
e-mail: hubentha@physik.uni-kassel.de

Present address:
R. Morarescu
Université de Mons Laboratoire Interfaces and Fluides Complexes, 20 Place du Parc, 7000 Mons, Belgium

1 Introduction

Highly ordered sub-diffraction sized nanostructures on surfaces generated in a parallel process are of enormous interest for a variety of applications in nanotechnology, e.g., for friction reduction [1], to study the static and dynamic properties of DNA [2], or to investigate cell differentiation on structured surfaces [3, 4]. To achieve such kind of nanostructures, light induced processes play an important role. Along these lines, ordered SiO_2, latex, or gold nanospheres on substrates have been illuminated with laser light [5–11]. For SiO_2 or latex spheres the focusing effect creates local fields on the substrate, which are high enough to overcome the ablation threshold of the substrate. Small round holes are generated underneath the spheres after applying a single laser pulse [6, 7, 9]. Elongated holes can also be created by varying the angle of incidence of the incoming laser light and using multi-pulses [8]. Another possibility to obtain elongated holes is to exploit the unique optical properties of noble metal nanoparticles. Briefly, the optical properties of noble metal nanoparticles are dominated by the excitation of localized surface plasmon polariton resonances, i.e., by a collective oscillation of the conduction band electrons [12, 13]. For simplicity, we refer to this kind of excitation as plasmon resonance or simply as plasmon. The excitation of a plasmon resonance is accompanied by a local field enhancement in the vicinity of the reversal points of the coherently oscillating electrons. Combining this effect with the focusing of the gold nanospheres, elongated holes have been generated on the underlying substrate in single

shot experiments [7, 14]. However, the most complex nanostructures have been generated using triangular nanoparticles [11, 15–17]. These nanoparticles have no focusing effect on the light and, hence, only the applied fluence and the near field distribution, which can be tuned by the polarization of the laser light, determine the shape of the ablation pattern. Along these lines, small holes [11, 15–17], nanochannels [15] and bone-like nanogrooves [16] have been generated.

However, detailed investigations, which modes contribute to the ablation process, are still lacking. In a recent publication by Kolloch et al. [18] either dipole-like ablation structures or quadrupole-like ablation structures have been observed for triangular nanoparticles of different sizes and significantly different plasmon resonances. In our presentation we demonstrate that, besides the strongly excited dipole mode, also higher order modes are *simultaneously* involved in the ablation process, which cause minor but clearly visible ablation structures in the substrate. Finally, we compare our results to the results obtained by Leiderer et al. [11]. The comparison reveals that the optical properties of the triangles have a significant influence on the generated ablation structures.

2 Experimental

2.1 Sample preparation

Regular arrays of triangular gold nanoparticles were prepared by means of nanosphere lithography [19–24], utilizing the drop coating method of Micheletto et al. [25]. Briefly, monodisperse latex nanospheres (Fa. Microparticles) with a diameter of 1390 nm have been assembled on fused silica plates with an edge length of 12 mm, which served as substrates. Under appropriate conditions, large monolayer areas of well-ordered latex nanospheres have been prepared, which were used as lithographic masks. Subsequently, a gold film with a thickness of 150 nm was deposited using a thermal evaporation chamber (Balzers BA 510) operating at a pressure of 10^{-6} Pa. Finally, the nanosphere masks were completely removed by sonicating the substrates for 3 minutes in dichloromethane, leaving behind large areas of highly ordered triangular gold nanoparticles. Details of the preparation can be found in the supplementary material of Ref. [16].

2.2 Laser treatment

To create the nanostructures on the substrate surface, the samples were irradiated under ambient conditions with single light pulses with a pulse duration of 35 fs (full width at half maximum) and a central wavelength of $\lambda = 790$ nm. The laser light was provided by an amplified Ti:Sapphire laser system (Femtolasers Femtopower Pro), coupled to a modified microscope set up. The light was expanded by a telescope system, to achieve a homogeneous illumination and a flat wave front. Afterwards, the laser light was focused by a Zeiss Epiplan 50x/0.5 NA objective on the sample surface. By placing a sample 20 µm ahead of the focus, the illuminated area on the sample surface was adjusted to 22 µm in diameter. The pulse energy has been adjusted by a motor driven gradient neutral density filter and was set to $E = 3.9$ µJ. Taking the Gaussian intensity profile of the laser light into account, the local fluence at the investigated area was $F = 1.36$ J/cm^2, i.e., well below the ablation threshold of fused silica (2 J/cm^2 [26, 27]). Irradiation of a sample has been performed with linearly polarized laser light at normal incidence. After applying a single pulse to one spot on a sample, it has been moved to a new position and another experiment has been performed. After irradiation, the samples were cleaned for 2 hours in aqua regia and subsequently sonicated for a few minutes in distilled water to remove residues of eventually remaining gold and ablated fused silica. Details of the laser set up and the laser treatment have been described elsewhere [16, 26].

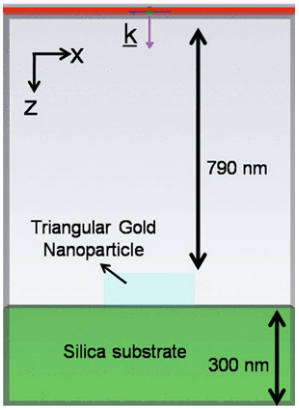

Fig. 1 Simulation setup for the nanoparticle calculations. On top and bottom, absorbing boundary conditions are used

2.3 Simulations

The time domain electromagnetic response for triangular nanoparticles is investigated separately, by using finite integration technique (FIT) using CST Microwave Studio.[1] In order to analyze the dependence of the modal excitation on the geometry, small and large triangular nanoparticles have been modeled.

The side length and thickness of the large (small) triangular nanoparticle are 320 nm (70 nm) and 100 nm (30 nm), respectively. For the simulations of the large triangular nanoparticles, smaller dimensions as compared to the experiment have been chosen to reduce the computational time. However, the simulations show all relevant features for

[1] www.cst.com.

the comparison with the experimental results. The computational domain of the system is shown in Fig. 1. The system is excited at normal incidence using a plane wave with different polarization directions, and traveling in the z-direction. Dirichlet and Neumann boundary conditions are applied at boundaries of the polarization directions for electric and magnetic fields, respectively. Open perfectly matched layer boundary conditions are applied along the z-direction of the computational domain. The time domain excitation signal is chosen to be a Gaussian modulated sine wave centered at a wavelength of 790 nm (379.7 THz) with a pulse duration of 35 fs (full width at half maximum). This translates into a bandwidth of approx. 13 THz (26 nm). The center wavelength and pulse duration are selected to be the same as the laser source in the experiment. The frequency dependent complex material properties of gold are represented by a Drude model fit to the available literature values [28]. The dielectric constant ϵ_r of silica is set to 2.08.

The aim of this study is to analyze the field enhancement due to plasmon–polariton modes at the triangle-silica interface for two different polarization directions. In addition, the power enhancement is computed from the ratio of time averaged power density at selected positions. Note that in all depicted simulation plots the mesh discretization around the metal-dielectric interface is smaller than 1 nm. However, for clarity the vectors in the electric field plots are interpolated to a much coarser grid. Finally, all presented plots are snap shots, taken at the time with the maximum field enhancement.

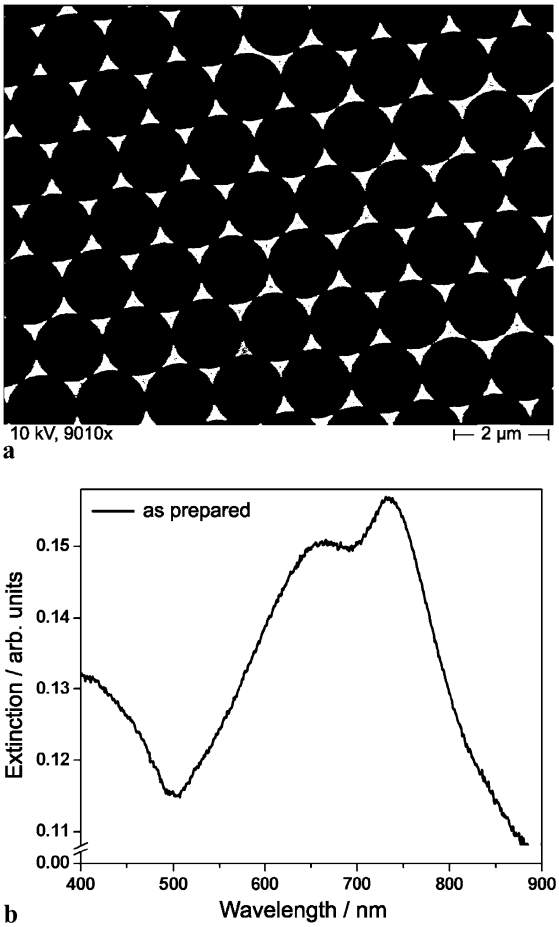

Fig. 2 (**a**) SEM image of the generated highly ordered triangular gold nanoparticles. (**b**) Extinction spectrum of the sample

3 Results

Figure 2(a) displays an SEM image of the generated gold nanoparticles on a fused silica substrate. It demonstrates that highly ordered triangular nanoparticles have been prepared. From the SEM image we obtain an edge length of the triangular nanoparticles of $L = (464 \pm 30)$ nm and a tip to tip distance between the nanoparticles of $D = (342 \pm 25)$ nm. Since the height cannot be extracted from the SEM image, additional ex situ AFM measurements have been performed (cf. Fig. 3(a)), which reveal a nanoparticle height of $H = (150 \pm 5)$ nm, as expected from the deposited amount of gold. The optical spectrum of a sample is depicted in Fig. 2(b). It shows one pronounced dipole plasmon resonance at $\lambda = 730$ nm, which can be attributed to the dipolar excitation of the triangular nanoparticles. The minor resonance at $\lambda = 650$ nm is caused by elongated nanoparticles, which have been simultaneously prepared on a different part of the sample due to a double layer mask. Since the spot for the extinction measurement is not limited to the triangular nanoparticles, both resonances are visible in the spectrum. However, for our experiments we focus solely on the triangular nanoparticles with a plasmon resonance at $\lambda = 730$ nm.

Before and in particular after illumination with laser light and cleaning of the sample, extensive AFM measurements have been performed. Figure 3 displays 3-dimensional AFM images of the sample. Image 3(a) depicts a single triangular gold nanoparticle before illumination. Figure 3(b) and (c) depict the generated nanostructures for a polarization direction of the laser light approximately along a common bisector and along the base of a triangle, respectively. Note that the triangular nanoparticles are completely removed from the fused silica substrate after a single laser shot, but their original position is clearly imprinted in the substrate. In the case of a polarization along the common bisector of the triangle (Fig. 3(b)), one major hole has been created. In contrast, if the polarization is along the base (Fig. 3(c)), two holes have been generated on the fused silica. The AFM analysis of a set of these holes yield a mean hole depth of $d = (20 \pm 3)$ nm and a mean hole width of $w = (100 \pm 5)$ nm. Besides the major holes, some minor, mainly linear sub-structures are observed, which do not necessarily appear at the tips rather than on the side edges of the

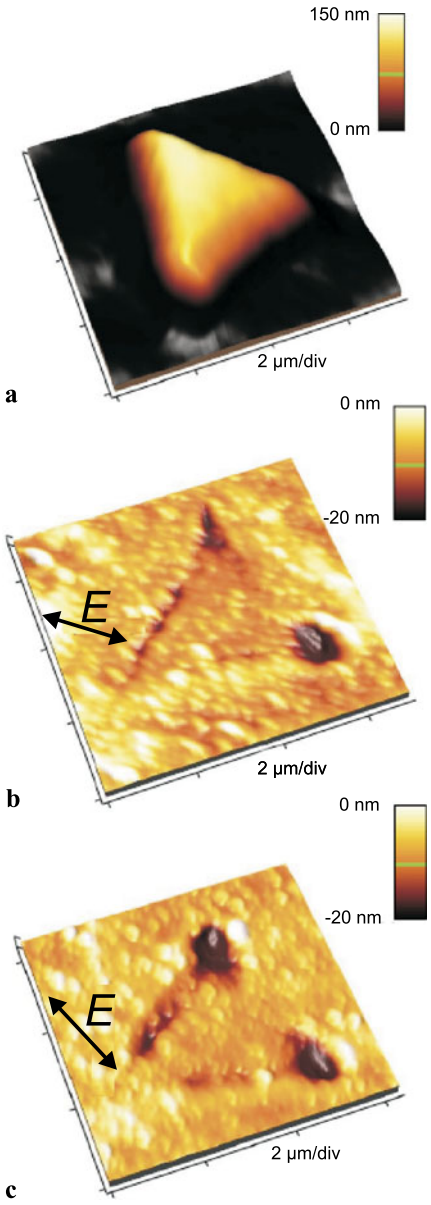

Fig. 3 (**a**): AFM image of a single triangular gold nanoparticle before laser treatment. (**b**) and (**c**): AFM images of the sample after illumination with a single linearly polarized laser pulse with a pulse duration of 35 fs. The *black arrows* indicate the polarization direction of the laser light

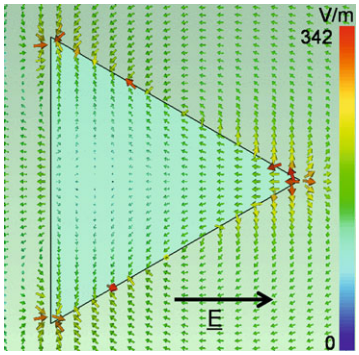

Fig. 4 Simulated electric field distribution for a metal triangle with side length of 320 nm, at the timestep of maximum field enhancement. The source polarization is in horizontal direction (as indicated)

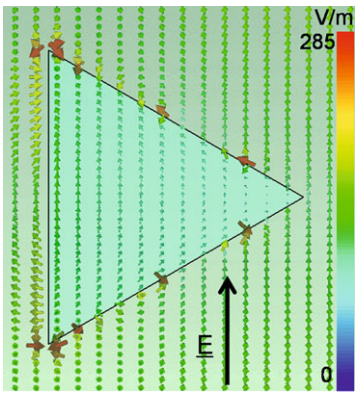

Fig. 5 Simulated electric field distribution for a metal triangle with side length of 320 nm, at the timestep of maximum field enhancement. The source polarization is parallel to the base of the triangle

former position of the triangles. This indicates that not only the dipole mode is involved, in fact, higher multipole modes contribute to the ablation. However, the effect due to higher multipoles is much weaker than for the dipole mode.

To explain the generated structures, extensive 3-dimensional simulations of the energy density of the local fields, using a finite integration technique in time domain, have been performed.

Figure 4 shows the field distribution at a time $t = 68.0$ fs after beginning of the excitation, for an incident pulse polarized along a common bisector of a large triangle. The maximum field is located at the triangle tip, which points in the direction of the polarization, while the other two tips show smaller field enhancements. But most importantly, field enhancements also occur along the base of the triangle, which is perpendicular to the polarization as well as on the other two side edges. The latter field enhancements originate from a multipolar excitation of higher order modes. The computed enhanced power at the triangle tip is 155 times higher compared to the power of the incident pulse.

The electric field distribution for a large triangle at $t = 64.2$ fs, illuminated with a polarization parallel to a base, is shown in Fig. 5. The snap shot shows that the field maximum is at the two tips parallel to the incident polarization, while the tip perpendicular to the polarization exhibits no field enhancement. For this configuration, the calculated power enhancement is 107. However, in this case relatively high field enhancements occur at the two side edges, which are not parallel to the polarization. As before, these fields are due to the excitation of higher order modes.

In addition to the simulations of the large triangular nanoparticles, simulations of the field enhancements of small triangles, with a side length of 70 nm and a height

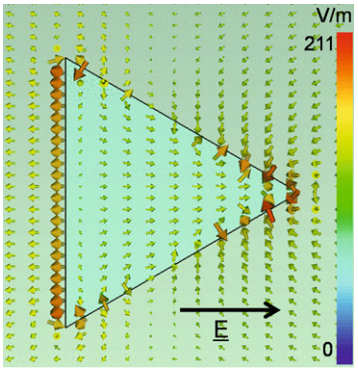

Fig. 6 Simulated electric field distribution for a metal triangle with side length of 70 nm, at the timestep of maximum field enhancement. The source polarization is in horizontal direction (as indicated)

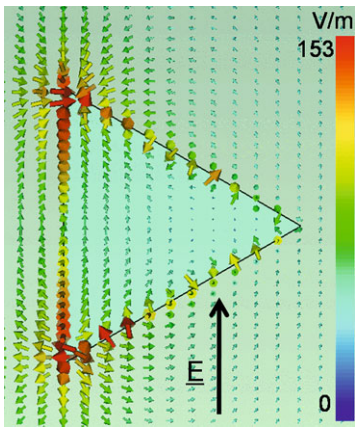

Fig. 7 Simulated electric field distribution for a metal triangle with side length of 70 nm, at the timestep of maximum field enhancement. The source polarization is parallel to the base of the triangle

of 30 nm have been performed, to demonstrate the influence of the nanoparticle size. Figure 6 depicts the electric field distribution at $t = 62.4$ fs for a polarization aligned along a common bisector of a small triangle. The plot shows that the field maximum is located at the triangle tip, which points in the direction of the polarization, but also strong fields at the other two tips occur. In addition, a smaller but significant field enhancement at the base of the triangle, which is perpendicular to the polarization, and on the side edges, take place. While the enhancement at the tips and the base is due to the dipolar excitation, the field enhancements along the side edges originate from a multipolar excitation of higher order modes. The computed enhanced power at the triangle tip is 32 times higher compared to the power of the incident pulse.

Figure 7 shows the electric field distribution of a small triangle at $t = 52.8$ fs for a polarization direction along the base of the triangle. For this configuration, the electric field has a maximum enhancement at the two tips, which are parallel to the polarization and is caused by the excitation of the dipole mode. In this case, the electromagnetic power is 17.5 times enhanced. However, also at the side edges of the nanoparticle field enhancements occur, due to excitation of higher order modes.

4 Discussion

First, we compare our experimental results with our simulations. The comparison between Figs. 3(b) and 4 shows a good agreement between the experiment and the simulations. The field maximum at the right tip in Fig. 4 is pronounced. Here, the highest power enhancement of 155 has been calculated, causing the major hole observed in the experiment. However, the agreement is not perfect, because in the experiment, the polarization was not exactly along the common bisector of the triangle. As a consequence, under the upper tip a minor hole appears, while under the left tip no hole is visible (cf. Fig. 3(b)). This non-symmetric characteristic can be explained by the not ideally oriented polarization, which was slightly tilted in the direction to the upper tip. Since in the simulations the polarization is exactly along the common bisector, the vector plot shows field enhancements on both nanoparticle tips, which are perpendicular to the polarization. In addition, a field enhancement along the base, which is perpendicular to the polarization, appears in the simulations (this effect is more pronounced for the small nanoparticles, cf. Fig. 6). The comparison to the experiment reveals that at this base, a clear linear ablation structure has been created. But most importantly, the vector plot also shows field enhancements at the side edges, which point to the strongly excited tip. These field enhancements are due to the excitation of higher order modes and create tiny linear ablation, which can be identified in Fig. 3(b). Thus, although experimental and theoretical conditions were not exactly the same, the results are in fair agreement and indicate that higher order modes play a role in the ablation process of larger triangles.

This indication that higher order modes play indeed an important role becomes more evident when comparing Fig. 3(c) with Fig. 5. For this configuration, i.e., polarization of the laser light is along the base of the triangle, we observe the same features in both images. Experimentally, two major holes under the tips that are oriented along the excited base are observed. In addition, minor ablation structures along the edges, which point to the tip, where no hole appeared, are clearly visible. This is in perfect agreement with our simulations, which show exactly at the tips, where we observe the holes, strong field enhancements due to the excitation of the dipole resonance. Furthermore, the simulations yield no field enhancement at the tip, which is oriented perpendicular to the polarization. In agreement with this result, no hole is observed under that tip. But most importantly, the simulations also show field enhancements along the side edges

of the triangle due to excitation of higher order modes. Although these fields are relatively weak, they are high enough to overcome the ablation threshold of the substrate and explain the observed minor ablation structures along the side edges.

Second, we compare the simulations for the small triangular nanoparticles with the large ones and with the results already published in Refs. [15, 16]. In general, the simulated field distribution of the small and large triangular nanoparticles are similar. This is not surprising, because in both cases the dipolar plasmon mode has been strongly excited. However, in contrast to the small triangular nanoparticle, for the large triangular nanoparticles the field enhancements due to the dipole mode and the multipole modes are well separated. Because of this separation, we observe minor ablation structures along the side edges of the large particles, which cannot be observed for small ones. This is confirmed by our previous publications [15, 16], in which experimentally the near field ablation of small triangular nanoparticles had been investigated. In addition, our simulations are in agreement with the simulations presented in Ref. [16] and, thus, perfectly explain the experimentally observed ablation pattern presented in Refs. [15, 16].

Third, we compare our results to the results published by Leiderer et al. [11]. The authors have investigated ablation structures caused by excitation ($\lambda_{\text{Laser}} = 800$ nm) of supported triangular gold nanoparticles, which have approximately the same lateral size as the investigated large nanoparticles here. At a first glance, the results seem to be contradictory, since for a polarization along the common bisector of the triangle, they observe two holes under the tips, which were perpendicular to the common bisector. In addition, no hole under the tip that points to the polarization direction of the laser light is observed [11]. In our experiments, similar ablation structures have been obtained with a polarization along a base of a triangle, i.e., rotated by 90° with respect to the polarization used by Leiderer et al. [11]. However, they used triangles with a height of only 25 nm. Hence, the aspect ratio, defined by the triangle height divided by the length of the common bisector, is much lower than in our experiment. Due to the low aspect ratio, the dipole plasmon resonance is strongly shifted to the infrared [12, 13]. Hence, Leiderer et al. did not excite the dipole resonance. As demonstrated in the paper by Kolloch et al. [18] they excite mainly the quadrupole mode, which results in a more complex field distribution of the nanoparticles. This explains the difference from our experiments, in which the dipole resonance has been strongly excited. In summary, the comparison of the results obtained by the Leiderer group and ours clearly demonstrates the crucial role of the optical properties of the nanoparticles on the field distribution of the nanoparticles. Only when the dipole mode is excited, a corresponding dipole-like ablation pattern, as presented in this publication, occurs. Note that Crozier et al. [29] have calculated that exciting triangular nanoparticles with a low aspect ratio with far infrared light results in a dipolar distribution of the near fields.

5 Summary and conclusions

Local near field assisted laser ablation exploiting the superior optical properties of triangular gold nanoparticles has been presented. We found that for large triangular gold nanoparticles, which strongly support higher order modes, pronounced ablation patterns occur. These patterns are significantly different from the dipole approximation. Although theoretically for all investigated nanoparticles the field enhancement due to higher order modes can be observed, experimentally only for the large nanoparticles the spatial separation is large enough to generate distinct ablation structures. In particular for laser pulses with a polarization parallel to the base of the triangle, ablation structures along the side edges occur that are well separated from the tip damage. This clearly proves ablation from field enhancements due to quadrupole or even higher order modes and demonstrated that for large nanoparticles both, dipolar and higher order modes contribute to the ablation process. Finally, we have shown, by comparison with the results of Leiderer et al. [11], that the optical properties of the excited nanoparticles play a crucial role for the generated nanopattern.

Acknowledgement R.M., F.T., and F.H. acknowledge financial support by the European Commission under contract MRTN-CT-2003-504233.

References

1. M. Zou, H. Wang, P.R. Larson, K.L. Hobbs, M.B. Johnson, O.K. Awitor, Ni nanodot-patterned surfaces for adhesion and friction reduction. Tribol. Lett. **24**, 137 (2006)
2. D.J. Bonthuis, C. Meyer, D. Stein, C. Dekker, Phys. Rev. Lett. **101**, 108303 (2008)
3. M.J. Dalby, N. Gadegaard, R. Tare, A. Andar, M.O. Riehle, P. Herzyk, C.D.W. Wilkinson, R.O.C. Oreffo, Nat. Mater. **6**, 997 (2007)
4. M.P. Lutolf, P.M. Gilbert, H.M. Blau, Nature **462**, 433 (2009)
5. G. Obara, Y. Tanaka, T. Miyanishi, M. Obara, Appl. Phys. A **102**, 551 (2011)
6. R. Denk, K. Piglmayer, D. Bäuerle, Appl. Phys. A **74**, 825 (2002)
7. N. Nedyalkov, T. Sakai, T. Miyanishi, M. Obara, Near field distribution in two dimensionally arrayed gold nanoparticles on platinum substrate. Appl. Phys. Lett. **90**, 123106 (2007)
8. W. Guo, Z.B. Wang, L. Li, D.J. Whitehead, B.S. Luk'yanchuk, Z. Liu, Appl. Phys. Lett. **90**, 243101 (2007)
9. M. Ulmeanu, M. Zamfirescu, L. Rusen, C. Luculescu, A. Moldovan, A. Stratan, R. Dabu, J. Appl. Phys. **106**, 114908 (2009)
10. D. Brodoceanu, L. Landström, D. Bäuerle, Appl. Phys. A **86**, 313 (2007)

11. P. Leiderer, C. Bartels, J. König-Birk, M. Mosbacher, J. Boneberg, Imaging optical near-fields of nanostructures. Appl. Phys. Lett. **85**, 5370 (2004)
12. F. Hubenthal, Noble metal nanoparticles: synthesis and applications, in *Comprehensive Nanoscience and Technology*, vol. 1, ed. by D.L. Andrews, G.D. Scholes, G.P. Wiederrecht (Academic Press, Oxford, 2011), pp. 375–435
13. U. Kreibig, M. Vollmer, *Optical Properties of Metal Clusters* (Springer, Berlin, 1995)
14. N.N. Nedyalkov, H. Takada, M. Obara, Nanostructuring of silicon surface by femtosecond laser pulse mediated with enhanced near-field of gold nanoparticles. Appl. Phys. A **85**, 163 (2006)
15. F. Hubenthal, R. Morarescu, L. Englert, L. Haag, T. Baumert, F. Träger, Parallel generation of nanochannels in fused silica with a single femtosecond laser pulse: exploiting the optical near fields of triangular nanoparticles. Appl. Phys. Lett. **95**, 063101 (2009)
16. R. Morarescu, L. Englert, B. Kolaric, P. Damman, R.A.L. Vallée, T. Baumert, F. Hubenthal, F. Träger, Tuning nanopatterns on fused silica substrates: a theoretical and experimental approach. J. Mater. Chem. **21**, 4076 (2011)
17. J. Boneberg, J. König-Birk, H.-J. Münzer, P. Leiderer, K.L. Shuford, G.C. Schatz, Optical near-fields of triangular nanostructures. Appl. Phys. A **89**, 299 (2007)
18. K. Ueno, H. Misawa, J. Boneberg, A.P.P. Leiderer, A. Kolloch, T. Geldhauser, Femtosecond and picosecond near-field ablation of gold nanotriangles: nanostructuring and nanomelting. Appl. Phys. A **104**, 793 (2011)
19. U.C. Fischer, H.P. Zingsheim, Submicroscopic pattern replication with visible light. J. Vac. Sci. Technol. **19**, 881 (1981)
20. J.C. Hulteen, D.A. Treichel, M.T. Smith, M.L. Duval, T.R. Jensen, R.P. Van Duyne, Nanosphere lithography: Size-tunable silver nanoparticle and surface cluster arrays. J. Phys. Chem. B **103**, 3854 (1999)
21. J. Anker, Y. Lin, M. Mrksich, R.P. Van Duyne, W.P. Hall, J. Modica, A conformation- and ion-sensitive plasmonic biosensor. Nano Lett. **11**, 1098 (2011)
22. C.-L. Chen, C.-C. Chen, D.P. Tsai, H.-P. Chiang, W.-C. Lin, S.-H. Huang, Controlling SERS intensity by tuning the size and height of a silver nanoparticle array. Appl. Phys. A **101**, 185 (2010)
23. E.K. Stone, W.L. Barnes, D.K. Polyushkin, E. Hendry, THz generation from plasmonic nanoparticle arrays. Nano Lett. **11**, 4718 (2011)
24. R. Morarescu, F. Träger, F. Hubenthal, Monitoring of molecule adsorption and molecular wire formation by in situ surface plasmon resonance spectroscopy. Int. J. Circuits Syst. Signal Process. **5**, 407 (2011)
25. R. Micheletto, H. Fukuda, M. Ohtsu, A simple method for the production of a two-dimensional, ordered array of small latex particles. Langmuir **11**, 3333 (1995)
26. L. Englert, B. Rethfeld, L. Haag, M. Wollenhaupt, C. Sarpe-Tudoran, T. Baumert, Opt. Express **15**, 17855 (2007)
27. M. Lenzner, J. Krüger, S. Sartania, Z. Cheng, C. Spielmann, G. Mourou, W. Kautek, F. Krausz, Phys. Rev. Lett. **80**, 4076 (1998)
28. P.B. Johnson, R.W. Christy, Optical constants of the noble metals. Journal of Physical Review B **6**(12) (1972)
29. K.B. Crozier, A. Sundaramurthy, G.S. Kino, C.F. Quate, J. Appl. Phys. **94**, 4632 (2003)